JOURNAL OF APPLIED ELECTROCHEMISTRY 25 (1995) 376–383

Electrodeposition and characterization of amorphous Fe–Ni–Cr-based alloys

J.-C. KANG, S. B. LALVANI*

Mechanical Engineering and Energy Processes, Southern Illinois University at Carbondale, Carbondale, IL 62901, USA

C. A. MELENDRES

Materials Science and Chemical Technology Divisions, Argonne National Laboratory, Argonne, IL 60439, USA

Received 10 February 1994; revised 2 July 1994

Electrodeposition of Fe–Ni–Cr-based alloys was investigated in a divided and undivided cell. Using formic acid (HCOOH) as a complexing agent, a chloride-hypophosphite solution was developed. Effects of composition on the morphology, structure, and corrosion behaviour of the alloys were studied. Effects of plating variables on composition of the alloys and current efficiency are also reported. Energy dispersive spectroscopy (EDS) and Auger electron spectroscopy (AES) were used to evaluate alloy composition. These alloys were determined to be amorphous by X-ray diffraction (XRD) and transmission electron microscopy (TEM). Scanning electron microscopy (SEM) photomicrographs were obtained of the surface of selected deposits. The corrosion behaviour of the alloys was studied in 0.9 wt % NaCl solution. The alloys containing phosphorus and carbon were found to be less active than those containing only phosphorus or carbon. The corrosion potential of Fe–Ni–Cr-based deposited alloys is more noble the higher the chromium content. Generally, Fe–Ni–Cr-based alloys exhibit a wide passivation range. Knoop hardness of the deposited alloys was determined. It is found that both phosphorus and carbon improved the Knoop hardness value of the deposited alloys.

1. Introduction

Electrodeposition of amorphous alloys has been widely studied in recent years. It was shown that amorphous Fe–P and Ni–P can be obtained when P is present in concentration greater than 12 at % [1, 2]. Feng *et al.* [3] have reported electrodeposition of amorphous Fe–Ni–Cr–P from two types of plating baths, namely sulfate-hypophosphite and chloride-hypophosphite baths, using glycine or trisodium citrate as a complexing agent for nickel and iron ions. However, the quality of the deposits produced was very poor, and the deposits were so thin that very little characterization was carried out. Lashmore *et al.* [4] deposited Ni–Cr-based alloys from an acidic electrolyte. Preliminary studies were conducted to determine a suitable plating electrolyte for Fe–Ni–Cr–P–C alloy deposition. A plating bath was tested to deposit Fe–Ni–Cr-based alloys. Formic acid was added in some cases, since it is known to enhance the appearance of the deposits. It also acted as the source of carbon. The effects of current density, temperature of plating electrolyte, and charge have been studied. Previous studies have shown that the use of a Nafion®† membrane resulted in lowering of the Cr content of the deposits [5, 6]. We believe that reduction of both Cr^{3+} and Cr^{6+} to Cr occurs at the cathode. Since Cr^{6+} is easier to deposit than Cr^{3+} [7, 8], chromium content of the deposits in the undivided cell was found to be greater than that obtained using a Nafion® membrane in a separated cell.

Naka *et al.* [9] claimed that alloys containing 8 at % or more Cr have good corrosion resistance. McBee *et al.* [10] reported that the surface film of Fe–Cr alloys changes from crystalline to amorphous as the Cr content is increased above 12.5 at %. This, in turn, improves corrosion resistance. In this study, the effects of composition on the corrosion behaviour, as well as hardness of the alloys, were obtained.

Iron–nickel–chromium–phosphorus–carbon alloys were deposited from the chloride solution listed in Table 1. In our previous investigation [6, 11], a sulfate electrolyte was used for Fe–Cr–P–C deposition. It was observed that chromium sulfate is somewhat more difficult to dissolve in aqueous solutions than the corresponding chloride salt; therefore, in the present investigation, a chloride solution for film deposition was adopted. Sodium hypophosphite was added as the source of phosphorus. Ammonium chloride is a complexant possibly in the high pH of the diffusion layer. Boric acid ($pK \sim 9$) served as a source of a borate complex at the pH values involved. Borate ion acts as an electron bridge. Formic acid was added, since it is known to enhance the appearance of the deposits [9, 14]. It also acted as source of

* Author to whom all correspondence should be addressed.
† Trademark of the DuPont Company

0021-891X

Table 1. Electrolyte composition for Ni–Cr-based alloys deposition

$FeCl_2$ (Ferrous Chloride)	10–20 g L^{-1}
$NiCl_2 \cdot 6H_2O$ (Nickel Chloride)	30–40 g L^{-1}
$CrCl_3 \cdot 6H_2O$ (Chromium Chloride)	100 g L^{-1}
NaH_2PO_2 (Sodium Hypophosphite)	0–20 g L^{-1}
NaBr (Sodium Bromide)	15 g L^{-1}
NH_4Cl (Ammonium Chloride)	50 g L^{-1}
H_3BO_3 (Boric Acid)	30 g L^{-1}
$Na_3C_6H_5O_7 \cdot 2H_2O$ (Sodium Citrate)	80 g L^{-1}
HCOOH (Formic Acid)	40 mL L^{-1}
Current density	30–40 A dm^{-2}
Charge	1000–2000 C
Temperature	Room–50 °C

carbon and as a complexing agent. Formate species buffers the pH in the cathode diffusion layer. Also included in the bath were ammonium bromide, an antioxidant, and sodium citrate, the complexing agent. The bath was operated at a pH of approximately 1.

In comparison with Feng's [3] deposition solution, our electrolyte contains formic acid and sodium citrate instead of glycine. Ammonium chloride and ammonium bromide are also included in this chloride-hypophosphite electrolyte. A cation selective Nafion® membrane separated the catholyte from the anolyte in our plating electrolyte.

2. Experimental methods

2.1. *Electrodeposition*

Electrodeposition was carried out under galvanostatic conditions from acidic electrolytes. A custom-made electrolysis cell with a platinum mesh anode was used during electrodeposition (Fig. 1). Gold foil in the shape of a rectangular strip was used as cathode. The gold substrates were polished with wet 600 grit SiC paper, then degreased with acetone, and rinsed with distilled water before being immersed in the electrolyte. The solution was stirred during plating with a magnetic stirring bar. The weight of the deposit was obtained from the difference in weight before and after deposition.

The electrolytes were prepared with singly distilled water and reagent grade chemicals. Nitrogen was bubbled through the electrolyte for 10 min prior to deposition in order to purge the solution of dissolved oxygen. A cation selective Nafion® membrane was used to separate the catholyte from the anolyte in most cases. The presence of the membrane resulted in more homogeneous and reproducible deposits. In a previous report [6], investigators used a Nafion® membrane so that Cr^{6+}, an oxidation product at the anode, was prevented from undermining the deposit produced at the cathode. Similar poor quality deposits in the absence of a cation selective membrane were observed for the synthesis of Cr–P–C thin films [12].

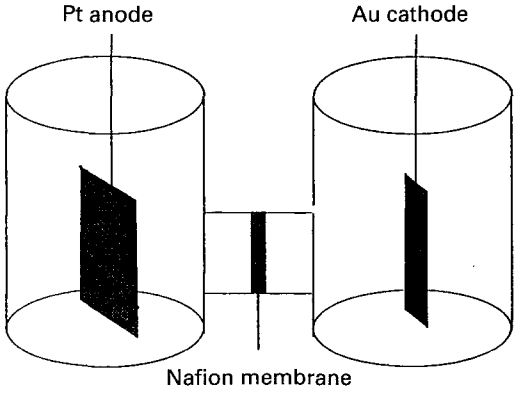

Fig. 1. The electrolysis cell used for electrodeposition.

2.2. *Characterization of deposits*

The alloy composition was determined by energy dispersive X-ray spectroscopy (EDS), performed in a JEOL JSM-35 scanning electron microscope (SEM) equipped with an energy dispersive X-ray analyser. A standardless X-ray microanalysis computer program, ZAP supplied by EG&G ORTEC was used to perform quantitative analysis. Carbon and oxygen could not be detected with the EDS unit. Auger electron spectroscopy (AES) was also used for compositional analysis for some selected samples. The structure of the deposits was determined by X-ray diffraction (XRD) with 2θ ranging from 5 to 70°. A Hitachi H-500H transmission electron microscope was used for transmission electron microscopy (TEM) analysis.

2.3. *Corrosion measurement*

Potentiodynamic polarization was carried out on selected deposits. The desired area of the deposit was exposed to a quiescent and deaerated solution of 0.9 wt % NaCl. The acidic electrolyte, 0.9 wt % NaCl, was prepared with distilled water and reagent grade chemical. Nitrogen was bubbled through the electrolyte for 10 min prior to the measurement to purge the solution of dissolved oxygen. A standard three-electrode electrolysis cell using a saturated calomel reference electrode (SCE) and a platinum-mesh counter electrode was used. Measurements were made with an EG&G Model 273 potentiostat/galvanostat. The corrosion potential (E_{corr}) and corrosion current (I_{corr}) were extrapolated from the experimental data using regression analysis software supplied with the EG&G Princeton Applied Research Model 342 corrosion unit. The corrosion measurements were performed according to the American Society of Testing and Materials (ASTM) G5-82 method. The specimen was immersed for 1 h before initiating polarization. The corrosion potential (E_{corr}) against time was recorded until E_{corr} reached a steady state before the scan was started. A potentiodynamic potential scan rate of 0.2 mV s^{-1} was used while current was sampled.

Table 2. Composition of Fe–Ni–Cr–C thin films as determined by EDS

Expt.	*Current density* /A dm^{-2}	*Charge* /C	*Composition*/at % *Fe*	*Ni*	*Cr*	*Current efficiency*/%	*Thickness* /μm*
1	10	500	62	10	28	41	25 (43)
2	15	500	48	8	44	35	22 (–)
3	15	300	48	6	46	32	12 (15)

The deposits were produced with Nafion® cation membrane. Deposition conditions as in Table 1 with 10 g L^{-1} $FeCl_2$, 40 g L^{-1} $NiCl_2$, 40 mL L^{-1} formic acid, and without NaH_2PO_2.
* Quantities in parenthesis represent the measured thickness.

3. Results and discussion

3.1. *Electrodeposition*

A modified electrolyte (Table 1) has been developed for electrodeposition of Fe–Ni–Cr–P–C alloys in this work. To investigate the effects of compositional elements on the morphology, structure, and corrosion behavior of the alloys, Fe–Ni–Cr–C, and Fe–Ni–Cr-P alloys were also deposited.

Ferrous alloys containing at least 12% Cr are known as stainless steel (SS), and they have corrosion resistance. When nickel is added, properties are further improved; for example, SS no. 304 $FeNi_{8-10.5}Cr_{18-20}C_{0.08}$ and SS no. 431 $FeNi_{1.25-2.5}Cr_{15-17}C_{0.2}$ have excellent corrosion resistance to acids [13]. In our experiments, it was possible to deposit Fe–Ni–Cr–C alloys on gold substrates from the electrolyte shown in Table 1 without the addition of NaH_2PO_2. Table 2 shows the effect of current density and charge on the composition, current efficiency, and thickness, as determined by EDS. The chromium content of the deposits was found to increase with the current density as expected, because the chromium deposition is known to occur at most electronegative potential of all the elements present in the electrolyte. Nickel, as well as iron content, decreased with the current density. The carbon content is not reported, since the EDS unit could not detect it. The current efficiency was higher, and deposits were thicker at lower current density than at higher current densities upon the passage of 500 C. Deposition is accompanied by hydrogen evolution, which results in a loss of current efficiency, especially at higher current density. Current efficiency of 41% for Fe–Ni–Cr–C deposited at 10 A dm^{-2} is significantly greater than that obtained for Fe–Cr–P–C amorphous deposits [6]. The current efficiency was about 32–35% at a current density of 15 A dm^{-2}. The deposit was found to be thicker with increase in the charge passed. The thickness of the deposits was calculated from the weight of the deposits and their composition. In the absence of the cation selective membrane, the deposits produced were thin and nonhomogenous. Thus, for film deposition, a divided cell must be used. The Fe–Ni–Cr–C deposits were found to contain oxygen and carbon by AES. Table 3 shows a comparison of compositional analysis between AES and EDS on a thin film deposited at 15 A dm^{-2} (expt. 3 in Table 2). Surface oxygen and carbon content of 46 and 6 at % were obtained while limiting values of 13 and 7 at % for the elements were recorded, respectively. This indicates that the surface of the deposit covered with an oxide layer; oxygen is present at depths of at least 50 nm in the deposit.

The composition of Fe–Ni–Cr–P alloys deposited without Nafion® membrane from the electrolyte in Table 1 with 20 g L^{-1} $FeCl_2$ and 10 g L^{-1} NaH_2PO_2 is shown in Table 4. The current density was varied from 5 to 10 A dm^{-2}, which resulted in an enhancement of the chromium content, as expected. No effect of increasing $NiCl_2$ from 30 to 40 g L^{-1} on the nickel content of expt. 7 was observed at the current density of 10 A dm^{-2}. Of all the types of alloy coating reported in this paper, good quality Fe–Ni–Cr–P could only be produced in an undivided cell.

Table 5 shows the composition of Fe–Ni–Cr–P alloys deposited without Nafion® membrane from the electrolyte in Table 1 with 40 g L^{-1} $NiCl_2$ and 20 g L^{-1} NaH_2PO_2. By lowering the concentration of $FeCl_2$ from 20 to 10 g L^{-1} the iron content was decreased from 73 to 65 at %.

With the addition of formic acid, Fe–Ni–Cr–P–C alloys can be produced from the chloride -hypophosphite solution shown in Table 1 with 10 g L^{-1} $FeCl_2$, 40 g L^{-1} $NiCl_2$, and 20 g L^{-1} NaH_2PO_2 in a divided cell. Table 6 shows the effect of current density on alloy composition and current efficiency of the deposition process. Both the chromium and nickel contents, as well as current efficiency, increased with current density, whereas the iron content decreased.

The effect of electrolyte temperature on the composition of Fe–Ni–Cr–P–C alloys at current densities of 30 and 40 A dm^{-2} is shown in Tables 8 and 9, respec-

Table 3. A comparison of compositional analysis between AES and EDS on an Fe–Ni–Cr–C thin film (expt. 3 in Table 2)

Element	*AES*/at % *Surface*	*Under 50 nm*	*EDS*/at %
Fe	19	45	48
Ni	8	6	6
Cr	21	29	46
C	6	7	–
O	46	13	–

Table 4. Composition of Fe–Ni–Cr–P thin films as determined by EDS

Expt.	*Current density*/A dm^{-2}	*Charge*/C	*Composition*/at %				*Thickness*/μm*	$NiCl_2$/g L^{-1}
			Fe	*Ni*	*Cr*	*P*		
4	5	200	87	6	5	2	7	30
5	7	200	84	3	7	6	14	30
6	10	72	67	4	13	16	–	30
7	10	100	66	5	14	15	12	40

The deposits were produced without Nafion® cation membrane. Deposition conditions as in Table 1 with 20 g L^{-1} $FeCl_2$ and 10 g L^{-1} NaH_2PO_2.

Table 5. Composition of Fe–Ni–Cr–P thin films as determined by EDS

Expt.	*Current density*/A dm^{-2}	*Composition*/at %				*Current efficiency*/%	*Thickness*/μm*	$FeCl_2$/g L^{-1}
		Fe	*Ni*	*Cr*	*P*			
8	5	73	3	7	17	–	20	20
9	5	65	6	10	19	22	14 (18)	10

* Quantities in parenthesis represent the measured thickness.
The deposits were produced without Nafion® cation membrane by passing a charge of 400 C. Deposition conditions as in Table 1 with 40 g L^{-1} $NiCl_2$ and 20 g L^{-1} NaH_2PO_2.

Table 6. Composition of Fe–Ni–Cr–P–C thin films as determined by EDS

Expt.	*Current density*/A dm^{-2}	*Composition*/at %				*Current efficiency*/%	*Thickness*/μm*
		Fe	*Ni*	*Cr*	*P*		
10	20	74	12	3	11	7	21
11	30	75	12	7	6	11	14
12	40	46	14	23	17	17	25 (28)

* Quantities in parenthesis represent the measured thickness.
The deposits were produced with Nafion® cation membrane by passing a charge of 1000 C. Deposition conditions as in Table 1 with 10 g L^{-1} $FeCl_2$, 40 g L^{-1} $NiCl_2$, 20 g L^{-1} NaH_2PO_2 and 40 mL L^{-1} formic acid.

tively. In both cases, the chromium content decreased with higher electrolyte temperature, whereas the nickel content increased. This is in full agreement with the previous study [3], where formic acid was not added to the plating solution. The current efficiency declined somewhat with temperature. Figure 2 contains SEM photomicrographs of the electrodeposits. Microcracks were observed on the $Fe_{62}Ni_{10}Cr_{28}C$ deposits, as is the case for chromium deposits. Small spherical nodules, characteristic of chromium are also present. When the carbon in the deposits was replaced by phosphorus, the microstructure did not look much different ($Fe_{67}Ni_4Cr_{13}P_{16}$). However, no microcracks were observed in a deposit containing both phosphorus and carbon ($Fe_{46}Ni_{14}Cr_{23}P_{17}C$), although the deposit contained a significant amount of chromium.

The effect of charge on the composition of alloys is reported in Table 10. The iron content decreased with the amount of charge passed, while both the chromium and phosphorus contents increased with the charge. There was no discernible influence of the charge passed on the nickel content and current efficiency. Thickness of the deposits, as expected, increased with the number of coulombs passed.

3.2. *Characterization of electrodeposits*

The X-ray diffraction patterns for most of the Fe–Ni–Cr–P–C deposits showed only a broad peak around 2θ of 43.35°. This broad peak suggests that the deposits are either amorphous or microcrystalline with crystal size below resolution for XRD of wavelength λ. It is interesting to note that although one of the deposits, $Fe_{48}Ni_6Cr_{46}C$, contains no phosphorus, the deposit also appears to be amorphous (Fig. 3). The amorphous structure may be attributed to the carbon content (which could not be determined by EDS). Data regarding the carbon content of the deposits are dis-

Table 7. A comparison of compositional analysis between AES and EDS on an Fe–Ni–Cr–P–C thin film (exp. 11 in Table 6)

Element	*AES*/at %		*EDS*/at %
	Surface	*Under 50 nm*	
Fe	38	62	75
Ni	9	9	12
Cr	7	2	7
P	7	19	6
C	5	4	–
O	34	4	–

Table 8. Composition of Fe–Ni–Cr–P–C thin films as determined by EDS

Expt.	*Bath temp/*°C	*Composition/*at %				*Current efficiency/*%	*Thickness/*μm
		Fe	*Ni*	*Cr*	*P*		
11	room	75	12	7	6	11	14
13	40	75	14	2	9	10	13
14	50	66	25	2	7	9	10
15	60	62	26	2	10	7	9

The deposits were produced at a current density of 30 A dm^{-2} with Nafion® cation membrane by passing a charge of 1000 C. Deposition conditions as in Table 1 with 10 g L^{-1} $FeCl_2$, 40 g L^{-1} $NiCl_2$, 20 g L^{-1} NaH_2PO_2 and 40 mL L^{-1} formic acid.

Table 9. Composition of Fe–Ni–Cr–P–C thin films as determined by EDS

Expt.	*Bath temp./*°C	*Composition/*at %				*Current efficiency/*%	*Thickness/*μm*
		Fe	*Ni*	*Cr*	*P*		
12	room	46	14	23	17	17	25 (28)
16	40	58	22	10	10	13	18 (27)
17	50	76	17	1	6	11	14 (18)
18	60	53	31	1	15	10	13 (15)

* Quantities in parenthesis represent the measured thickness.
The deposits were produced at a current density of 40 A dm^{-2} with Nafion® cation membrane by passing a charge of 1000 C. Deposition conditions as in Table 1 with 10 g L^{-1} $FeCl_2$, 40 g L^{-1} $NiCl_2$, 20 g L^{-1} NaH_2PO_2 and 40 mL L^{-1} formic acid.

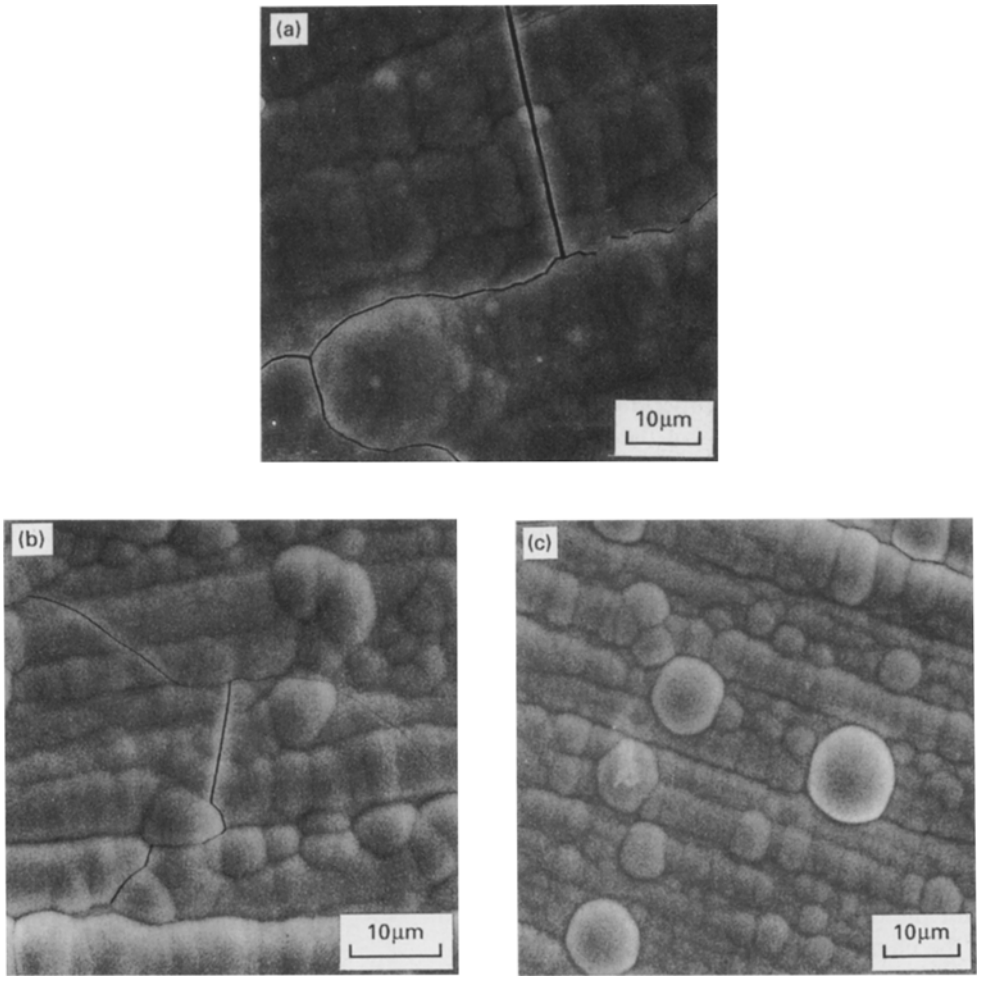

Fig. 2. SEM photomicrographs of the surface of Fe–Ni–Cr–C deposits: (a) $Fe_{62}Ni_{10}Cr_{28}$ C (X1200) (expt. 1, Table 2); (b) $F_{67}Ni_4Cr_{13}P_{16}$ (X1200) (expt. 6, Table 4); and (c) $Fe_{46}Ni_{14}Cr_{23}P_{17}C$ (X1200) (expt. 12, Table 9).

Table 10. Composition of Fe–Ni–Cr–P–C thin films as determined by EDS

Expt.	*Charge/C*	*Composition/at %*				*Current efficiency/%*	*Thickness/μm*
		Fe	*Ni*	*Cr*	*P*		
11	1000	75	12	7	6	11	14
19	1500	69	13	9	9	10	20
20	2000	54	13	10	23	12	37

The deposits were produced at a current density of 30 A dm^{-2} and room temperature with Nafion® cation membrane. Deposition conditions as in Table 1 with 10 g L^{-1} $FeCl_2$, 40 g L^{-1} $NiCl_2$, 20 g L^{-1} NaH_2PO_2 and 40 mL L^{-1} formic acid.

cussed below. Transmission electron microscopy (TEM) was also performed on the samples. The selected area diffraction patterns (SADPs) of the deposit (i.e., $Fe_{48}Ni_6Cr_{46}C$) and that of $Fe_{67}Ni_4Cr_{13}P_{16}$ are shown in Fig. 4. The SADPs of both deposits are essentially identical. They consist of a prominent diffuse ring and some faint outer rings. The bright field images were found to be generally uniformly mottled, indicating an amorphous structure (figures not included).

The Fe–Ni–Cr–P–C deposits were found to contain carbon and oxygen, as determined by Auger electron spectroscopy (AES). The surface of the deposit was found to be covered with an oxide layer, as indicated in the AES depth profile (Fig. 5). This oxide layer is about 20 nm in thickness and is probably a mixture of chromium oxide and some iron oxides. Tables 3 and 7 show a comparison of compositional analysis between AES and EDS techniques. The surface oxygen content of the deposits is high; however, the bulk oxygen content (13%) of the deposit reported in Table 3 is much greater than the corresponding oxygen content (4%) of the deposit reported in Table 7. It is also interesting to note that the chromium content of the former deposit is significantly larger than that of the latter. Thus, it appears that oxygen associated with chromium is incorporated into the coatings during the electrodeposition step.

3.3 *Corrosion*

Potentiodynamic polarization was carried out in quiescent and deaerated solution of 0.9 wt % NaCl. The alloys containing phosphorus and carbon were found to be less active based on the corrosion data provided in Table 11. This result is in agreement with Naka *et al.*'s [14] investigations, which showed that the combination of P and C results in an extremely high corrosion resistance in Fe–Cr-based amor-

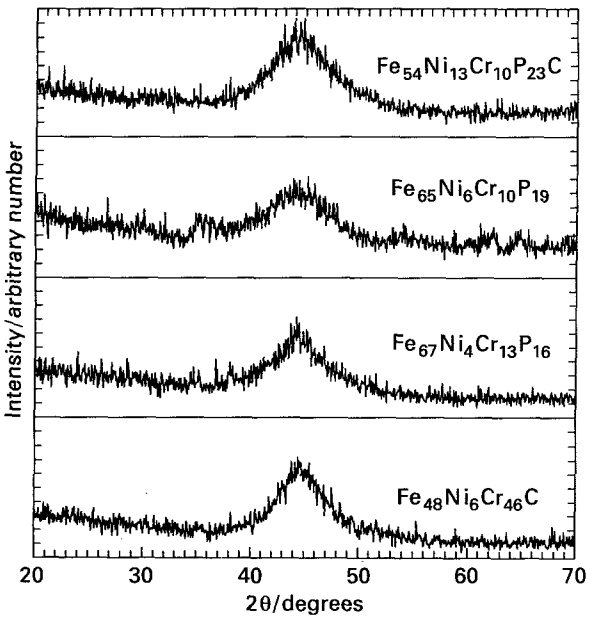

Fig. 3. The X-ray diffraction (XRD) pattern of amorphous $Fe_{48}Ni_6Cr_{46}C$, $Fe_{67}Ni_4Cr_{13}P_{16}$, $Fe_{65}Ni_6Cr_{10}P_{19}$ and $Fe_{54}Ni_{13}Cr_{10}P_{23}C$ deposits.

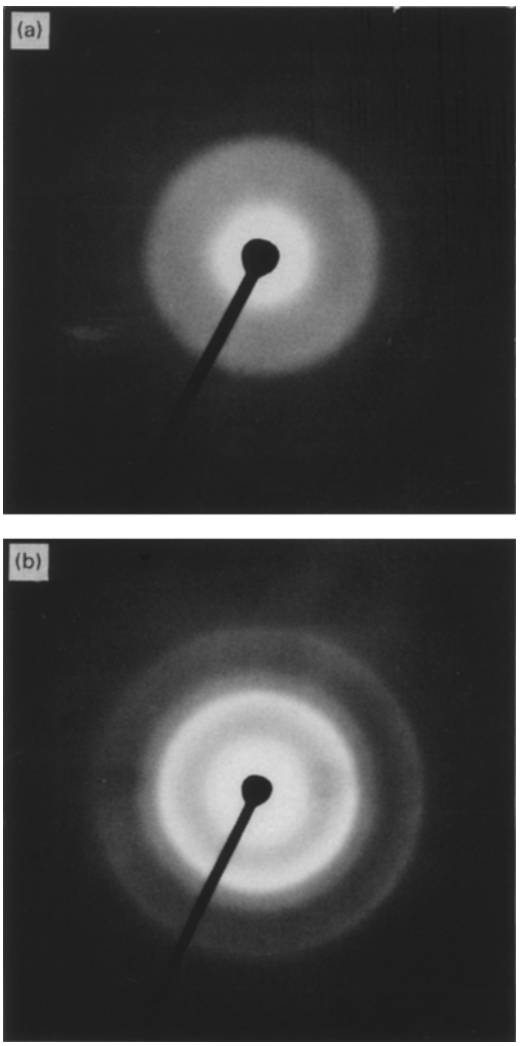

Fig. 4. TEM SADPs of amorphous (a) $Fe_{48}Ni_6Cr_{46}C$ and (b) $Fe_{67}Ni_4Cr_{13}P_{16}$.

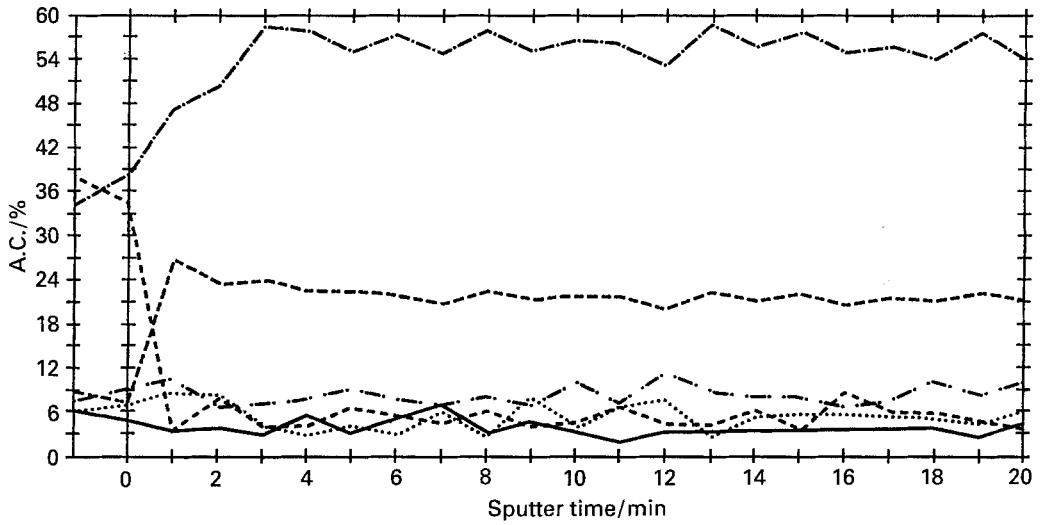

Fig. 5. Depth profile of composition determined by AES for an Fe–Ni–Cr–P–C deposit (expt. 11, Table 6). Sputter rate: ~ 70 A min^{-1}. Key: (–·–·–) Fe; (– – –) P; (—·—·—) Ni; (·····) Cr; (- - -) O; (——) C.

phous alloys. It should be noted that a low corrosion current alone is not in itself an indicator of how well the alloy will protect the substrate.

Figure 6 shows the potentiodynamic polarization curves of Fe–Ni–Cr–P and Fe–Ni–Cr–P–C deposits. The anodic behaviour of all coatings in 0.9 wt % NaCl shows a passivation range. Confirmation that amorphous Fe–Ni alloys containing more than 8 at % Cr have extremely high corrosion resistance can be found in the literature [14]. The corrosion potential is more noble with higher chromium content. This is in agreement with previous investigations [6, 11], where corrosion behaviour was measured in 0.5 M HCl solution. The Flade potentials of Fe–Ni–Cr–P and Fe–Ni–Cr–P–C deposits were found to be as high as 1.4 V vs SCE.

3.4. *Hardness measurement*

The Knoop hardness test was employed for the deposited alloy coatings. Measurements were taken on a cross-sectional area of each specimen and the average and standard deviations were calculated for each. With a small loading (10 g), extra care was taken in selecting the areas for the measurement and ensuring a perpendicular indentation to the surface. Such a loading gives small indenter impressions resulting in greater scatter in the measurements, thus requiring more measurements be made for adequate statistical treatment of the data. Each of the measurements taken was close to the centre of the coating and parallel to the surface, to avoid any edge effects.

Table 12 compares the effect of each element on the hardness readings of the deposited alloys. As reported in previous investigation [11], both carbon and phosphorus affect the hardness dramatically. The presence of C in the Fe–Ni–Cr-based alloys results in a significant improvement of the hardness. Alloys with higher chromium content have higher hardness, since chromium is known as a hard element. With similar chromium content, phosphorus also has influence on the hardness value of the deposited alloys, as seen by comparing $Fe_{66}Ni_5Cr_{10}P_{15}$ with $Fe_{65}Ni_6Cr_{10}P_{19}$, and $Fe_{76}Ni_{17}Cr_1P_6C$ with $Fe_{53}Ni_{31}Cr_1P_{15}C$. Among all deposited alloys, Fe–Ni–Cr–C has the highest hardness, apparently because of the relatively high chromium and carbon content.

Table 11. A comparison of corrosion data for selected alloys in 0.9 wt % NaCl

*Expt**	*Alloys*	E_{corr} /mV vs SCE	I_{corr} /μA cm^{-2}
6	$Fe_{67}Ni_4Cr_{13}P_{16}$	−281	1.62
9	$Fe_{65}Ni_6Cr_{10}P_{19}$	−602	0·09
20	$Fe_{54}Ni_{13}Cr_{10}P_{23}C$	−545	0.12

* Corresponding to previous Tables.

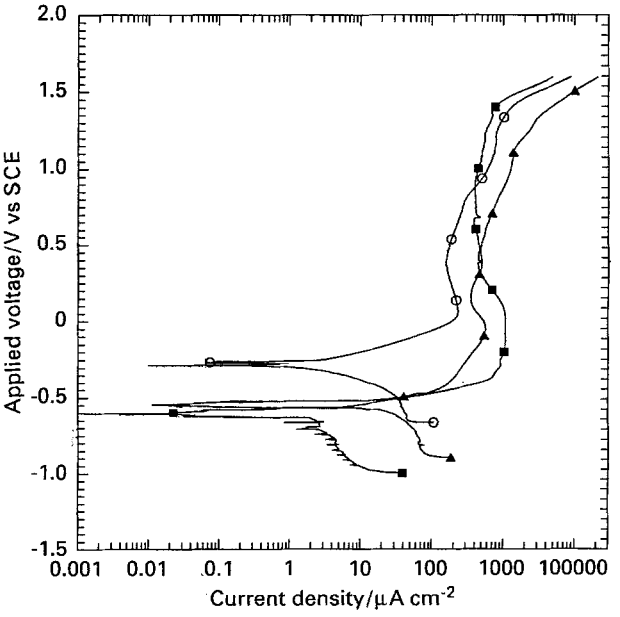

Fig. 6. Potentiodynamic polarization curves of Fe–Ni–Cr–P and Fe–Ni–Cr–P–C deposits in 0.9 wt % NaCl. Key: (○—○) $Fe_{67}Ni_4Cr_{13}P_{16}$; (■—■) $Fe_{65}Ni_6Cr_{10}P_{19}$; and (▲—▲) $Fe_{54}Ni_{13}Cr_{10}P_{23}C$.

Table 12. A comparison of Knoop hardness data for selected alloys

*Expt.**	*Alloys*	*Hardness* /HK	*Deviation* /HK
1	$Fe_{62}Ni_{10}Cr_{28}C$	511	±11
3	$Fe_{48}Ni_6Cr_{46}C$	521	±40
4	$Fe_{87}Ni_6Cr_5P_2$	311	±31
5	$Fe_{84}Ni_3Cr_7P_6$	304	±22
7	$Fe_{66}Ni_5Cr_{10}P_{15}$	225	±33
9	$Fe_{65}Ni_6Cr_{10}P_{19}$	312	±80
12	$Fe_{46}Ni_{14}Cr_{23}P_{17}C$	391	±25
16	$Fe_{58}Ni_{22}Cr_{10}P_{10}C$	351	±13
17	$Fe_{76}Ni_{17}Cr_1P_6C$	326	±40
18	$Fe_{53}Ni_{31}Cr_1P_{15}C$	407	±41

* Corresponding to previous tables.

4. Conclusions

A new electrolyte for electrodeposition of amorphous Fe–Ni–Cr-based thin films has been tested. Alloy deposition can be carried out from a divided cell (with membrane) with and without addition of formic acid. A lower temperature is recommended in order to increase the chromium content and current efficiency. Phosphorus and carbon were found to improve the hardness value of the deposits, as well as their corrosion resistance. Higher chromium content results in increasing the corrosion potential, which, in turn, enhances corrosion resistance. Among all the alloys studied, the amorphous Fe–Ni–Cr–P–C alloys exhibit the widest passivation region.

References

[1] St. Vitkova, M. Kjuchukova and G. Raichevski, *J. Appl. Electrochem.* **18** (1988) 673.
[2] A. Brenner, D. E. Couch and E. K. Williams, *J. Res. Natl. Bur. Std.* **44** (1950) 109.
[3] L.-Q. Feng and M.-X. Shen, Proceedings of the 8th International Congress on Metal Corrosion, vol. 2 (1981) pp.1121.
[4] D. S. Lashmore, I. Weisshaus and K. W. Pratt, *Plat. Surf. Finish.* **73** (1986) 48.
[5] P. K. Ng, T. E. Mitchell, I. E. Locci and A. A. Ruiz, *J. Mater. Res.* **4** (1989) 300.
[6] J.-C. Kang and S. B. Lalvani, *J. Appl. Electrochem.* **22** (1992) 787.
[7] F. A. Lowerheim, Editor, 'Modern Electroplating', 3rd edn, John Wiley & Sons, New York (1974).
[8] A. Brenner, 'Electrodeposition of Alloys', vol. 1, Academic Press, New York (1963).
[9] M. Naka, K. Hashimoto and T. Masumoto, *Corrosion-NACE*, **32**(4), (1976) 146.
[10] C. L. McBee and Kruger, *Electrochim. Acta* **17** (1972) 1337.
[11] S. B. Lalvani and J.-C. Kang, *J. Mater. Sci. Lett.* **11** (1992) 835.
[12] B. A. DeNeve and S. B. Lalvani, *J. Appl. Electrochem.* **22** (1992) 341.
[13] 'ASM Metals Handbook', vol. 3, 9th edn (1980).
[14] M. Naka, K. Hashimoto and T. Masumoto, *J. Non-Cryst. Solids* **28** (1978) 403.